nature medicine

Vessel co-option mediates resistance to anti-angiogenic therapy in liver metastases

Sophia Frentzas[1,2,11], Eve Simoneau[3,11], Victoria L Bridgeman[1,11], Peter B Vermeulen[1,4,11], Shane Foo[1,11], Eleftherios Kostaras[1], Mark R Nathan[1], Andrew Wotherspoon[2], Zu-hua Gao[3], Yu Shi[3], Gert Van den Eynden[4], Frances Daley[5], Clare Peckitt[2], Xianming Tan[6], Ayat Salman[3], Anthoula Lazaris[3], Patrycja Gazinska[7], Tracy J Berg[1], Zak Eltahir[2], Laila Ritsma[8], Jacco van Rheenen[8], Alla Khashper[3], Gina Brown[2], Hanna Nyström[4,9], Malin Sund[9], Steven Van Laere[4], Evelyne Loyer[10], Luc Dirix[4], David Cunningham[2,12], Peter Metrakos[3,12] & Andrew R Reynolds[1,12]

The efficacy of angiogenesis inhibitors in cancer is limited by resistance mechanisms that are poorly understood. Notably, instead of through the induction of angiogenesis, tumor vascularization can occur through the nonangiogenic mechanism of vessel co-option. Here we show that vessel co-option is associated with a poor response to the anti-angiogenic agent bevacizumab in patients with colorectal cancer liver metastases. Moreover, we find that vessel co-option is also prevalent in human breast cancer liver metastases, a setting in which results with anti-angiogenic therapy have been disappointing. In preclinical mechanistic studies, we found that cancer cell motility mediated by the actin-related protein 2/3 complex (Arp2/3) is required for vessel co-option in liver metastases *in vivo* and that, in this setting, combined inhibition of angiogenesis and vessel co-option is more effective than the inhibition of angiogenesis alone. Vessel co-option is therefore a clinically relevant mechanism of resistance to anti-angiogenic therapy and combined inhibition of angiogenesis and vessel co-option might be a warranted therapeutic strategy.

The concept that metastases can become vascularized through sprouting angiogenesis, in a process stimulated by vascular endothelial growth factor-A (VEGFA), prompted the clinical development of anti-angiogenic agents, including the VEGFA-targeted antibody bevacizumab[1,2]. Bevacizumab combined with chemotherapy (bev–chemo) can extend progression-free and/or overall survival in several cancer types, including metastatic colorectal cancer (CRC)[3,4]. Indeed, bev–chemo is now an approved treatment for many different cancer types, including metastatic CRC. Despite this success, the survival benefit achieved with the addition of bevacizumab to chemotherapy is modest, measured in terms of only months. Moreover, in other cancer types, including metastatic breast cancer, anti-angiogenic therapy has yet to demonstrate a survival benefit for patients[5,6]. The mechanisms that limit the therapeutic efficacy of anti-angiogenic therapy for patients are still poorly understood.

More recently, it has emerged that metastases can also vascularize by the nonangiogenic mechanism of vessel co-option, a process whereby cancer cells, instead of inducing new vessel growth, incorporate pre-existing vessels from surrounding tissue[7–10]. Anti-angiogenic agents (including bevacizumab) were designed to target sprouting angiogenesis, not the process of vessel co-option. Accordingly, vessel co-option has been suggested as a potential mechanism of resistance to anti-angiogenic therapy[6,9–11]. Here we provide evidence that vessel co-option is a clinically relevant mechanism of resistance to anti-angiogenic therapy in liver metastases. Moreover, we show that, in an *in vivo* metastasis model, combined inhibition of angiogenesis and vessel co-option is more effective than the inhibition of angiogenesis alone.

RESULTS

Replacement growth pattern liver metastases respond poorly to bevacizumab

The liver is the most common site of involvement in metastatic CRC, and surgical removal of CRC liver metastases (CRCLMs) is now recommended practice for eligible patients[12]. Careful histopathological examination of human CRCLMs has shown that these tumors can present with three different histopathological growth patterns (HGPs): the desmoplastic HGP, the pushing HGP or the replacement HGP

[1]Tumour Biology Team, The Breast Cancer Now Toby Robins Research Centre, The Institute of Cancer Research, London, UK. [2]The Royal Marsden Hospital, London, UK. [3]McGill University Health Centre, Royal Victoria Hospital–Glen Site, Montreal, Quebec, Canada. [4]Translational Cancer Research Unit, Gasthuiszusters Antwerpen Hospitals St. Augustinus, Antwerp, Belgium. [5]Breast Cancer Now Histopathology Core Facility, The Royal Marsden Hospital, London, UK. [6]Lineberger Comprehensive Cancer Center, University of North Carolina, Chapel Hill, North Carolina, USA. [7]Breast Cancer Now Unit, Guy's Hospital, King's College London School of Medicine, London, UK. [8]Cancer Genomics Center the Netherlands–Hubrecht Institute–Royal Netherlands Academy of Arts and Sciences & University Medical Centre Utrecht, Utrecht, the Netherlands. [9]Department of Surgical and Perioperative Sciences, Umeå University, Umeå, Sweden. [10]University of Texas MD Anderson Cancer Center, Houston, Texas, USA. [11]These authors contributed equally to this work. [12]Co-senior authors. Correspondence should be addressed to A.R.R. (andrew.reynolds@icr.ac.uk), P.M. (peter.metrakos@mcgill.ca) or D.C. (David.Cunningham@rmh.nhs.uk).

Received 24 March; accepted 9 September; published online 17 October 2016; doi:10.1038/nm.4197

(**Fig. 1a** and **Supplementary Fig. 1**)[8,13]. These growth patterns have distinct histopathological features and utilize different mechanisms to obtain a vascular supply. In the desmoplastic HGP, the cancer cells are separated from the normal liver parenchyma by a capsule of desmoplastic stroma. In the pushing HGP, no desmoplastic capsule is present, but the cancer cells do not infiltrate the hepatic plates of the adjacent liver parenchyma. Instead, the tumor compresses the hepatic plates of the adjacent liver parenchyma. For both of these growth patterns, angiogenesis is used to obtain a vascular supply for the tumor. However, in metastases with a replacement HGP, the cancer cells infiltrate the hepatic plates of the liver parenchyma and co-opt pre-existing sinusoidal vessels, rather than promoting angiogenesis[8,13,14]. Although bevacizumab was not designed to target vessel co-option, no study has addressed whether the replacement growth pattern (where vessel co-option occurs) is associated with resistance to bevacizumab in liver metastases.

To address this question, we took advantage of the fact that some patients with metastatic CRC receive pre-operative therapy with bev–chemo in the months that precede surgical removal of CRCLMs[15–17]. We evaluated the HGPs and the pathological response to therapy in 59 CRCLMs resected from 33 patients who had been treated pre-operatively with bev–chemo at The Royal Marsden Hospital (RM) by examining H&E-stained liver resection specimens (**Fig. 1b**) (for patient details, see **Supplementary Fig. 2** and **Supplementary Table 1**). Given that CRCLMs can present with a mixture of HGPs[13], the percentages of desmoplastic, pushing and replacement HGPs were quantified in each lesion. To measure response to therapy, the pathological response in each lesion was scored in quartiles (>75%, 50–75%, 25–49% or <25% viable tumor). Lesions with <25% viable tumor were considered to be good responders, whereas lesions with ≥25% viable tumor were considered to be poor responders.

Notably, lesions with a substantial (≥50%) replacement component were significantly enriched in the group of lesions classified as poor responders when compared to the group of lesions classified as good responders (**Fig. 1b**; $P < 0.001$). By contrast, lesions with a substantial (≥50%) desmoplastic component were significantly enriched in the group of lesions classified as good responders when compared to the group of lesions classified as poor responders (**Fig. 1b**; $P < 0.001$). Similar results were obtained when the same analysis was repeated using only the single largest lesion from each individual (**Supplementary Fig. 3**). In a univariate analysis of other clinical variables, only the HGP showed a statistically significant association with pathological response (**Supplementary Table 2**).

Some examples of the lesions examined for this analysis are shown in **Figure 1c–e**. In **Figure 1c**, a lesion scored as >75% viable with an HGP score of 100% replacement is shown; note the close contact between tumor cells and liver parenchyma in the infiltrative replacement growth pattern (arrows). In **Figure 1d**, a lesion scored as <25% viable with an HGP score of 100% desmoplastic is shown; note that the entire circumference of the tumor is desmoplastic and well encapsulated (arrowheads). In this lesion, a large central area of infarct-like necrosis (ILN), indicative of a strong treatment response, is labeled (asterisks). In **Figure 1e**, a lesion scored as <25% viable that has a mixed growth pattern (79% desmoplastic, 19% replacement, 2% pushing) is shown; note the presence of a desmoplastic rim at the periphery of the tumor (arrowheads) that surrounds a large central area of ILN (asterisks). However, at the periphery of the tumor, two viable nodules with a replacement HGP can be seen (arrows).

To validate the association between the HGPs and pathological response to therapy, we next examined a larger series of 128 CRCLMs from 59 individuals who were treated pre-operatively with bev–chemo at the McGill University Health Centre (MUHC) (for patient details, see **Supplementary Fig. 4** and **Supplementary Table 3**). Again, lesions with ≥50% replacement HGP were significantly enriched in the poorly responding group of lesions (**Fig. 1f**; $P < 0.001$), whereas lesions with ≥50% desmoplastic HGP were significantly enriched in the group of lesions classified as good responders (**Fig. 1f**; $P < 0.001$). Similar results were obtained when the same analysis was repeated using only the single largest lesion from each patient (**Supplementary Fig. 5**). In a univariate analysis, the HGP was the strongest predictor of pathological response (**Supplementary Table 4**).

Included in these analyses were both patients who presented with a solitary liver metastasis and individuals who presented with multiple liver metastases. Therefore, we also examined a subset of 29 patients who presented with a single lesion only (pooled from the RM and MUHC cohorts). In this subset, the HGP was also correlated with pathological response (**Supplementary Fig. 6**). Univariate and multivariate analyses of 181 lesions from 90 individuals (pooled from the RM and MUHC cohorts) were also performed to determine clinical characteristics associated with a good pathological response (**Supplementary Table 5**). Only the HGPs showed a statistically significant association with pathological response: the replacement HGP was associated with a lower probability of obtaining a good pathological response (odds ratio (OR) = 0.07, 95% CI 0.03–0.16, $P < 0.0001$ in univariate and OR = 0.06, 95% CI 0.03– 0.15, $P < 0.0001$ in multivariate). By contrast, the desmoplastic HGP was associated with a higher probability of obtaining a good pathological response (OR = 15.06, 95% CI 6.32–35.87, $P < 0.0001$ in univariate and OR = 15.92, 95% CI 6.76–37.51, $P < 0.0001$ in multivariate). Taken together, these data demonstrate that the replacement HGP is associated with a poor pathological response to bev–chemo in CRCLMs.

To provide an alternative measure of treatment response, we also evaluated radiological response in the lesions from the RM patients. Recently published guidelines recommend that response to bev–chemo should be evaluated using computed tomography (CT) scans according to novel morphological response criteria, which correlate better with outcome than conventional response evaluation criteria in solid tumours (RECIST)[12,18,19]. In brief, to measure morphological response, the appearance of each lesion on both the pre- and post-treatment scans was scored as belonging to one of three morphology groups: group-1, group-2 or group-3 (see Online Methods for details on how these groups were defined). An optimal response (OR) was recorded if the lesion changed from group-3 or group-2 to group-1 after treatment; a partial response (PR) if the lesion changed from group-3 to group-2 after treatment; and an absent response (AR) if the lesion either did not change group or went from group-2 to group-3 after treatment. Lesions scored as AR were considered to be poor responders, whereas lesions scored as PR or OR were considered to be good responders.

We found that lesions with ≥50% replacement HGP were significantly enriched in the poor-response group, according to these morphological response criteria (**Fig. 2**; $P = 0.006$). Similar results were obtained when the same analysis was repeated using only the single largest lesion from each patient (**Supplementary Fig. 7**). These data provide independent verification that CRCLMs with a replacement HGP respond poorly to bevacizumab. However, no correlation between the HGP and response to therapy was observed when using RECIST-based criteria as a measure of response (**Supplementary Fig. 8**).

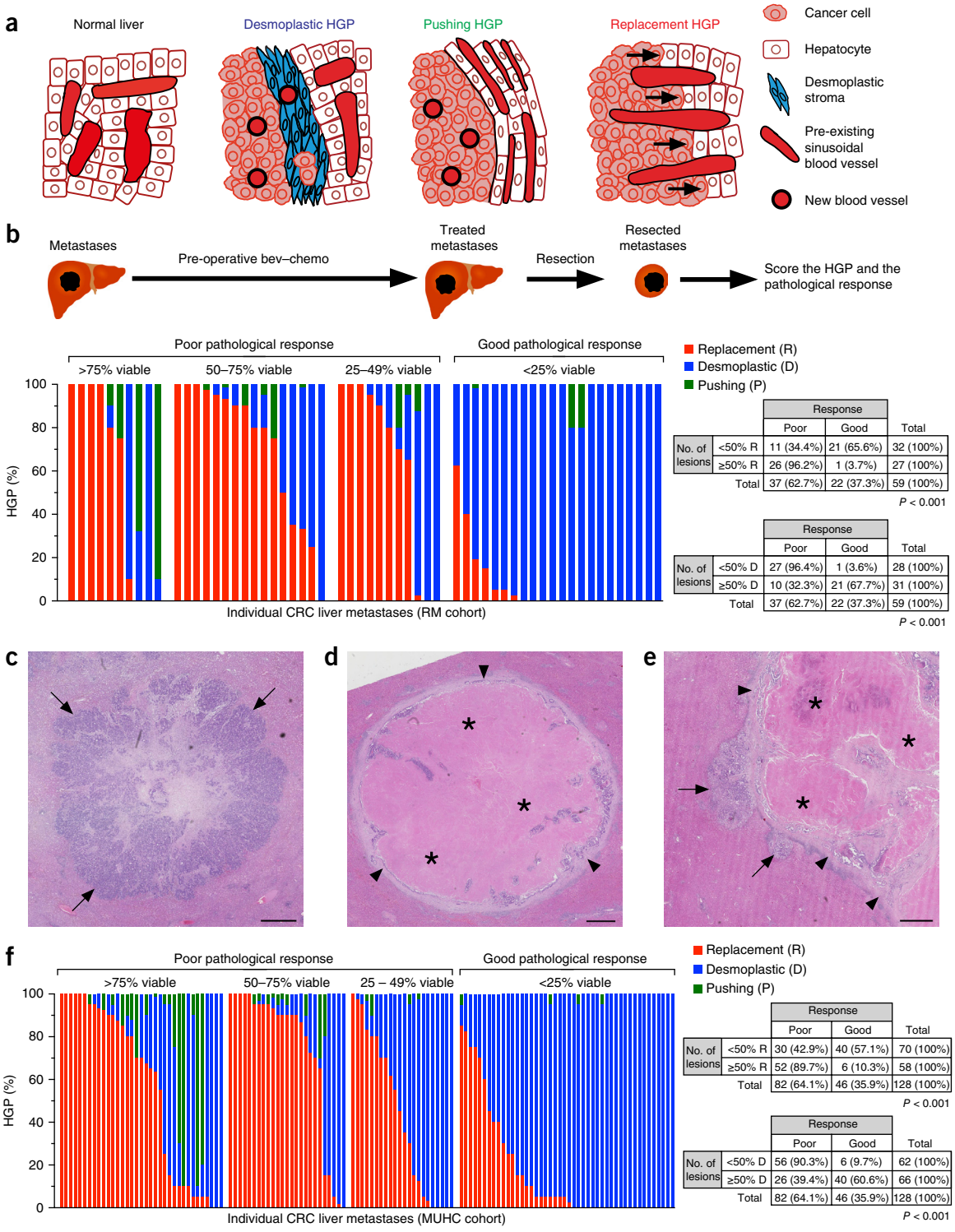

Figure 1 Correlation between HGP and pathological response in patients treated pre-operatively with bevacizumab. (**a**) The morphology of the normal liver and the morphology of the tumor–liver interface in liver metastases with a desmoplastic, pushing or replacement HGP. Black arrows indicate the direction in which cancer cells infiltrate the liver parenchyma in the replacement HGP. (**b**) The HGPs and the pathological response to bev–chemo were scored in 59 CRCLMs from 33 individuals treated pre-operatively with bev–chemo at RM. The % HGP (replacement, desmoplastic, pushing) scored in each individual lesion is shown, and the data are grouped by pathological response score: >75%, 50–75%, 25–49% or <25% viable tumor. The median number of lesions examined per patient was 1 (range = 1–4 lesions per patient). (**c**–**e**) Examples of H&E-stained lesions from the RM cohort are shown. Arrows, replacement HGP areas; arrowheads, examples of desmoplastic HGP areas; asterisks, areas of infarct-like necrosis. (**f**) The HGPs and the pathological response to bev–chemo were scored in 128 CRCLMs from 59 patients treated with bev–chemo at MUHC. The % HGP (replacement, desmoplastic, pushing) scored in each individual lesion is shown, and the data are grouped by pathological response score: >75%, 50–75%, 25–49% or <25% viable tumor. The median number of lesions examined per patient was 2 (range = 1–12 lesions per patient). The χ^2-test was used to determine statistical significance (see 2 × 2 contingency tables in **b** and **f**). Scale bars, 1 mm.

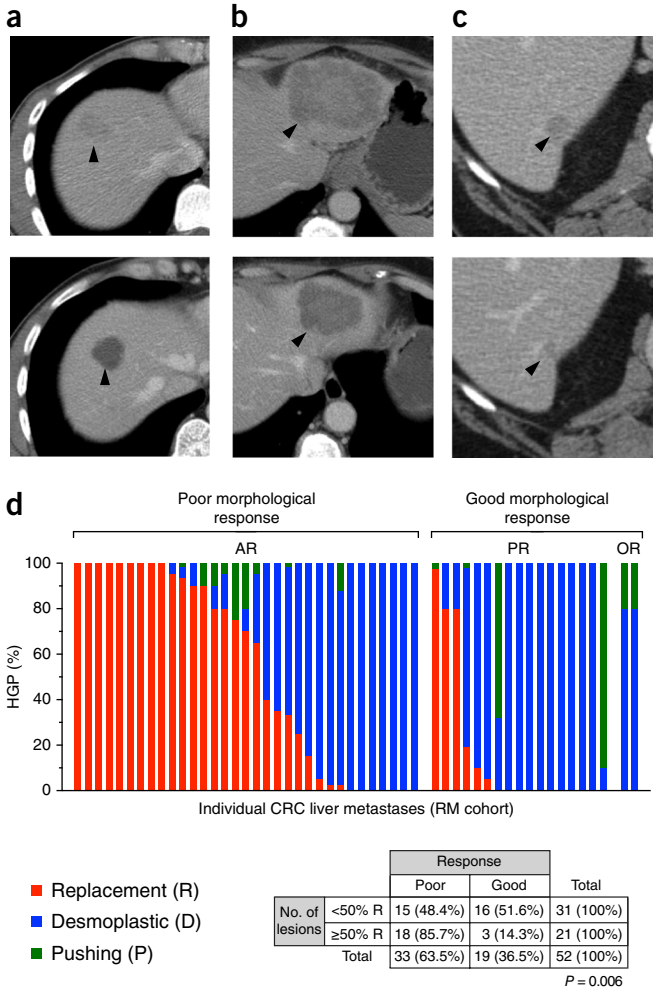

		Response		
		Poor	Good	Total
No. of lesions	<50% R	15 (48.4%)	16 (51.6%)	31 (100%)
	≥50% R	18 (85.7%)	3 (14.3%)	21 (100%)
	Total	33 (63.5%)	19 (36.5%)	52 (100%)

$P = 0.006$

Figure 2 Liver metastasis HGP correlates with morphological responses on CT in patients treated pre-operatively with bevacizumab. (**a**–**c**) CT scans of liver metastases of patients treated pre-operatively with bev–chemo. Examples of optimal (OR), partial (PR) and absent (AR) morphological responses are shown. (**a**) OR: a lesion in liver segment VII (arrowhead) is scored as group-3 before treatment (top) and as group-1 after four cycles of bevacizumab in combination with CAPOX (bottom). (**b**) PR: a lesion in liver segment II (arrowhead) is scored as group-3 before treatment (top) and as group-2 after four cycles of bevacizumab in combination with CAPOX (bottom). (**c**) AR: a lesion in liver segment VI (arrowhead) is scored as group-3 both before treatment (top) and after six cycles of bevacizumab in combination with FOLFIRI (bottom). (**d**) Morphological responses and HGPs were scored in 52 liver metastases from 31 patients treated pre-operatively with bev–chemo at RM. The % HGP scored in each individual lesion (replacement, desmoplastic, pushing) is shown. Lesions are grouped according to response: AR, PR or OR. Lesions scored as AR were classified as poor responders, whereas those scored as PR or OR were classified as good responders. The median number of lesions examined per patient was 1 (range = 1–4 lesions per patient). The χ^2 test was used to determine statistical significance (see 2 × 2 contingency table in **d**).

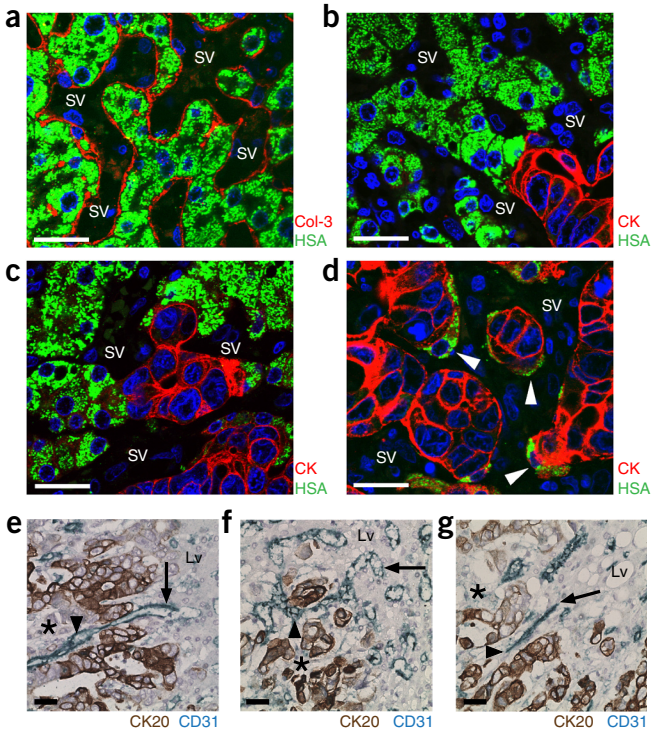

Figure 3 Cancer cells infiltrate the hepatic plates and co-opt sinusoidal blood vessels in the replacement HGP. (**a**) A representative image of normal liver, stained for HSA (green) to detect hepatocytes and collagen-3 (col-3, red) to detect liver sinusoidal blood vessels (SV). (**b**–**d**) Staining for pan-cytokeratin to detect cancer cells (CK, red) and hepatocytes (HSA, green) at the tumor–liver interface (**b**,**c**) and within the tumor mass (**d**) in a replacement HGP liver metastasis of colorectal cancer. Displaced hepatocytes are marked (arrowheads). (**e**–**g**) Staining for cytokeratin 20 (CK20, brown) to identify cancer cells and CD31 to identify blood vessels (blue) in replacement HGP liver metastases of colorectal cancer. Arrows and arrowheads indicate liver sinusoidal blood vessels, where one end of the vessel is physically located in the liver parenchyma (arrows) and the other end is surrounded by cancer cells (arrowheads). Asterisks, tumor. Lv, normal liver. SV, sinusoidal blood vessel. Scale bars, 25 μm.

Cancer cells infiltrate the hepatic plates and co-opt sinusoidal blood vessels in the replacement growth pattern

We next investigated the mechanism of tumor vascularization in replacement HGP CRCLMs by examining, in detail, the relationship between cancer cells and the normal liver in this growth pattern. In normal liver, staining for hepatocyte-specific antigen (HSA) identified hepatocytes within the hepatic plates, and collagen-3 staining identified the intervening sinusoidal blood vessels (SVs; **Fig. 3a**). In the replacement HGP, co-staining for cancer cells (pan-cytokeratin) and hepatocytes (HSA) demonstrated that invading cancer cells line up neatly with hepatocytes within the hepatic plates at the tumor–liver interface (**Fig. 3b**). Replacement of hepatocytes by invading cancer cells was clearly observed (**Fig. 3c**). Behind the invasive tumor front, near complete replacement of hepatocytes by cancer cells was evident, and flattened displaced hepatocytes were observed frequently at the edge of cancer cell nests (**Fig. 3d**). However, cancer cells clearly respected the spaces occupied by SVs (**Fig. 3b**–**d**). Therefore, in the replacement growth pattern of liver metastasis, cancer cells invade the liver parenchyma, replace hepatocytes and co-opt SVs.

Further evidence for vessel co-option was obtained by staining for the endothelial marker CD31. In the replacement HGP, SVs in which one end of the vessel was physically located in the normal liver (arrows in **Fig. 3e**–**g**) and the other end was embedded in the tumor (arrowheads in **Fig. 3e**–**g**) were frequently observed, consistent with the concept that these tumors co-opt SVs as they infiltrate the liver parenchyma (see also **Supplementary Fig. 9a**,**b**). However, this phenomenon was not observed in the desmoplastic or pushing HGPs (**Supplementary Fig. 9c**–**f**). In addition, co-staining of tumors for CD31 and HSA demonstrated that tumor vessels at the

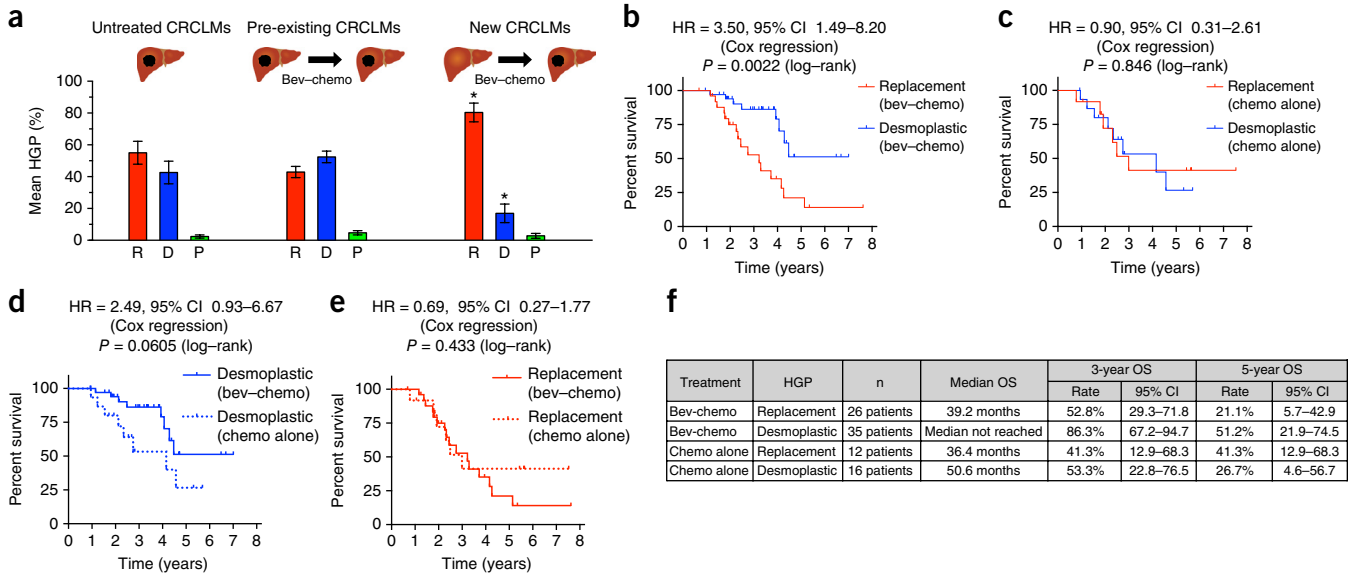

Treatment	HGP	n	Median OS	3-year OS		5-year OS	
				Rate	95% CI	Rate	95% CI
Bev-chemo	Replacement	26 patients	39.2 months	52.8%	29.3–71.8	21.1%	5.7–42.9
Bev-chemo	Desmoplastic	35 patients	Median not reached	86.3%	67.2–94.7	51.2%	21.9–74.5
Chemo alone	Replacement	12 patients	36.4 months	41.3%	12.9–68.3	41.3%	12.9–68.3
Chemo alone	Desmoplastic	16 patients	50.6 months	53.3%	22.8–76.5	26.7%	4.6–56.7

Figure 4 The replacement HGP occurs in progressive disease and is associated with a poor outcome in patients treated with bevacizumab. (**a**) The % replacement (R), % desmoplastic (D) and % pushing (P) HGP per lesion ± s.e.m. in untreated CRCLMs (left; $n = 32$ lesions from 19 MUHC patients), HGPs in pre-existing CRCLMs (middle; $n = 128$ lesions from 59 MUHC patients) and HGPs in new CRCLMs (right; $n = 35$ lesions from 13 MUHC patients). (**b**) Kaplan–Meier estimates of OS for 61 MUHC patients treated pre-operatively with bev–chemo who were stratified into two groups: predominant replacement HGP (26 patients) or predominant desmoplastic HGP (35 patients). (**c**) Kaplan–Meier estimates of OS for 28 MUHC patients treated pre-operatively with chemotherapy alone who were stratified into two groups: predominant replacement HGP (12 patients) or predominant desmoplastic HGP (16 patients). (**d**) Kaplan–Meier estimates of OS for 51 MUHC patients with a predominant desmoplastic HGP who were stratified into two groups: desmoplastic HGP treated with bev–chemo (35 patients) or desmoplastic HGP treated with chemotherapy alone (16 patients). (**e**) Kaplan–Meier estimates of OS for 38 MUHC patients with a predominant replacement HGP who were stratified into two groups: replacement HGP treated with bev–chemo (26 patients) or replacement HGP treated with chemotherapy alone (12 patients). (**f**) Median, 3-year and 5-year OS for patients in each group. The Kruskall–Walls test (**a**) or the log–rank test (**b**–**e**) were used to determine statistical significance. Hazard ratios were calculated using Cox regression. $*P < 0.001$.

periphery of replacement HGP metastases were often still physically associated with hepatocytes, providing more evidence that these vessels are co-opted sinusoidal vessels and not newly formed vessels (**Supplementary Fig. 10a**,**b**). However, this association was not observed in the desmoplastic or pushing HGPs (**Supplementary Fig. 10c**,**d**). Taken together, these findings strongly suggest that although the replacement HGP CRCLMs co-opt pre-existing sinusoidal vessels, desmoplastic and pushing HGP CRCLMs do not.

Prevalence of the replacement HGP in progressive disease after bevacizumab treatment

Unfortunately, patients can progress after treatment with bev–chemo by developing new CRCLMs[20]. Here we define new CRCLMs as lesions observed in the liver after the initiation of bev–chemo treatment that were not evident on pre-treatment scans. In the analyses of treatment response described above (**Fig. 1**), we examined only resected CRCLMs that had been detected on pre-treatment scans before treatment initiation, and we specifically excluded any newly appearing CRCLMs, even if they were resected. Given that new CRCLMs occur despite bev–chemo treatment, these new lesions might be representative of progressive disease that is resistant to bev–chemo. In the MUHC case series, 35 newly appearing CRCLMs from 13 patients were available for assessment (for patient details, see **Supplementary Table 6**). We compared the HGPs in these new CRCLMs with two control groups from the MUHC cases: pre-existing CRCLMs, i.e., lesions resected from patients treated with bev–chemo that had been detected on pre-treatment scans before treatment initiation (128 CRCLMs from 59 individuals; for patient details, see **Supplementary Table 3**); and untreated CRCLMs, i.e., lesions resected from MUHC patients who had not received any pre-operative therapy (32 CRCLMs from 19 individuals; for patient details see **Supplementary Table 7**). The percentage of tumor scored as having a replacement HGP was significantly increased in new CRCLMs, as compared to the CRCLMs in both control groups ($P < 0.001$; **Fig. 4a**). Concomitantly, there was a significant decrease in the desmoplastic HGP in new CRCLMs when compared to both control groups ($P < 0.001$; **Fig. 4a**). These data provide evidence for an increased prevalence of the replacement HGP in patients who progress after treatment with bev–chemo.

Patients with replacement HGP liver metastases receive less clinical benefit from bevacizumab

We next examined whether the HGP of liver metastasis could affect the clinical benefit achieved with anti-angiogenic therapy in terms of patient survival (**Fig. 4b**–**f**). Kaplan–Meier estimates of overall survival (OS) were calculated for a cohort of 62 individuals from MUHC who were treated pre-operatively with bev–chemo between 2008 and 2014 and for a cohort of 29 individuals from MUHC who were treated pre-operatively with chemotherapy alone during the same period. Patients were stratified into groups on the basis of their liver metastasis growth pattern: predominant replacement HGP, predominant desmoplastic HGP or predominant pushing HGP (see Online Methods for details on how these groups were defined).

In the bev–chemo cohort, individuals with predominant desmoplastic HGP had a significantly better OS, as compared to the predominant replacement HGP patients (HR = 3.50, 95% CI 1.49–8.20, $P = 0.0022$; **Fig. 4b**). These data suggest that patients with replacement HGP liver metastases receive less clinical benefit from treatment with bevacizumab than patients with desmoplastic HGP liver metastases.

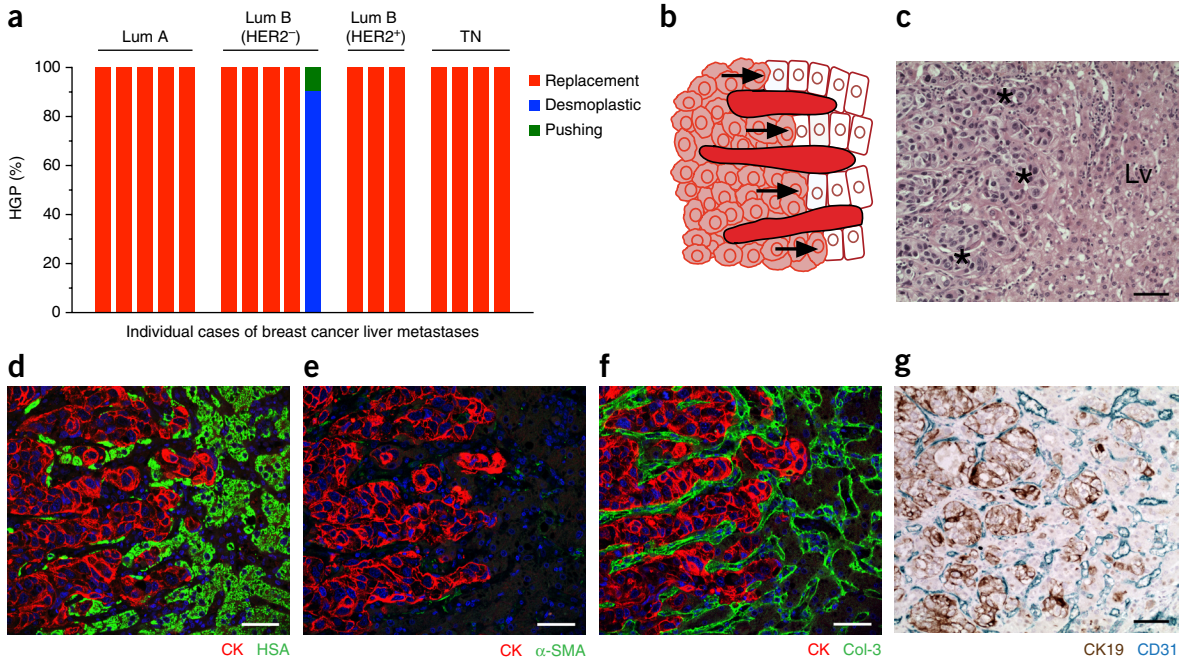

Figure 5 The replacement HGP predominates in breast cancer liver metastases. (**a**) The % HGP (replacement, desmoplastic, pushing) scored in breast cancer liver metastases (BCLMs) from 17 patients is shown. The cases are grouped by intrinsic subtype of breast cancer: Lum A, luminal A; Lum B (HER2$^-$), luminal B HER2 negative; Lum B (HER2$^+$), luminal B HER2 positive; TN, triple negative. (**b**–**g**) Morphology of the replacement growth pattern of BCLMs. Tumor–liver interface in the replacement HGP (**b**); black arrows indicate the direction in which cancer cells infiltrate the liver parenchyma in the replacement HGP. The tumor–liver interface in a human BCLM sample, as visualized by H&E staining (**c**). Asterisk, cancer cells; Lv, normal liver. Breast cancer cells infiltrate the liver parenchyma and replace hepatocytes in BCLM, as visualized by co-staining for HSA to label hepatocytes and pan-cytokeratin (CK) to label cancer cells (**d**). Absence of a desmoplastic stroma at the tumor–liver interface in BCLM, as visualized by co-staining for α–smooth muscle actin (α-SMA) to label fibroblasts and CK to label cancer cells (**e**). The vascular architecture of the adjacent liver is preserved at the tumor–liver interface in BCLM, as visualized by co-staining for collagen-3 (col-3) to label sinusoidal vessels and CK to label cancer cells (**f**). The infiltrative pattern of tumor growth facilitates vessel co-option in BCLM, as visualized by co-staining for CD31 to label blood vessels and cytokeratin 19 (CK19) to label cancer cells (**g**). Scale bars, 50 μM.

The HGP was the only variable that showed a statistically significant association with OS in univariate and multivariate analyses (**Supplementary Table 8**). In addition, both 3-year and 5-year OS were longer for patients with desmoplastic HGP than for those with replacement HGP in the bev–chemo cohort (**Fig. 4f**). However, in the cohort treated with chemotherapy only, no significant difference in OS was observed between individuals with desmoplastic HGP and replacement HGP (HR = 0.90, 95% CI 0.31–2.61, $P = 0.846$; **Fig. 4c**).

Using the same data set, we examined whether a difference in OS exists between individuals with desmoplastic HGP who received chemotherapy alone and those who received bev–chemo. The difference in OS was not statistically significant (HR = 2.49, 95% CI 0.93–6.67, $P = 0.0605$; **Fig. 4d**). We also examined whether a difference in OS exists between patients with replacement HGP who received chemotherapy alone and those who received bev–chemo. Again, the difference in OS was not significant (HR = 0.69, 95% CI 0.27–1.77, $P = 0.433$; **Fig. 4e**).

Patients with a predominant replacement HGP had similar clinical characteristics when compared to those with a predominant desmoplastic HGP (**Supplementary Table 9**), but the interval between the last dose of therapy and resection tended to be longer in the replacement HGP group than in the desmoplastic HGP group (median interval of 83 d for replacement versus 62 d for desmoplastic HGP patients, $P = 0.030$). We also examined whether differences existed between the clinical characteristics of the patients treated with bev–chemo and those treated with chemotherapy alone (**Supplementary Table 10**). The cohorts were similar except that a larger proportion of patients received irinotecan-based chemotherapy in the bev–chemo cohort when compared to the chemotherapy-alone cohort (19% of bev–chemo patients versus 10.3% of chemotherapy-alone patients; $P = 0.019$).

When stratifying patients on the basis of their liver metastasis HGP, only two patients were designated in the predominant pushing group (one patient treated with bev–chemo and one patient treated with chemotherapy alone), and these patients were not included in the Kaplan–Meier analysis (**Fig. 4b–e**). Both of these patients had a poor outcome, as they died within 2 years of diagnosis of liver metastasis. This is consistent with the findings of a previous study, which showed that the pushing HGP is an independent predictor of poor overall survival at a 2-year follow-up[21]. It is therefore possible that the pushing HGP of CRCLMs is associated with a poor outcome regardless of treatment modality.

The replacement HGP is prevalent in breast cancer liver metastases

Thus far, disappointing results have been obtained with anti-angiogenic therapy in metastatic breast cancer[5,6]. Therefore, we also examined the HGP in breast cancer liver metastasis samples, obtained from 17 patients, by examining H&E-stained tissue sections (for patient details, see **Supplementary Table 11**). The replacement HGP was predominant in 16 of 17 cases examined, with only one individual presenting with a predominant desmoplastic HGP (**Fig. 5a**). Further histopathological characterization of replacement HGP

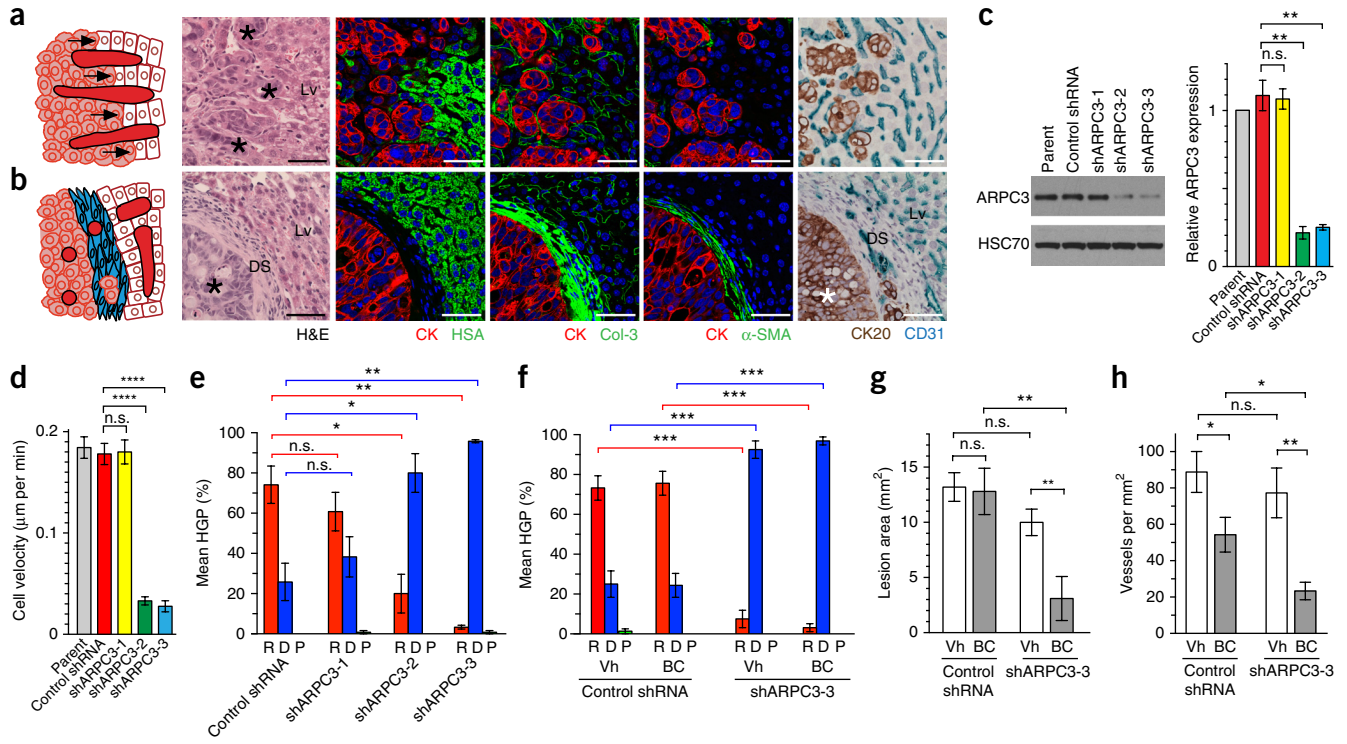

Figure 6 Inhibition of vessel co-option and angiogenesis is more effective than targeting angiogenesis alone. (**a**,**b**) Areas of replacement (**a**) and desmoplastic (**b**) HGP are shown in a preclinical (HT29 cell line) orthotopic model of advanced liver metastasis. Staining shown is for: H&E, CK and HSA, CK and col-3, CK and α-SMA or cytokeratin 20 (CK20) and CD31, as indicated. Asterisk, cancer cells; DS, desmoplastic stroma; Lv, normal liver. Black arrows indicate the direction in which cancer cells infiltrate the liver parenchyma in the replacement HGP. (**c**,**d**) Characterization of parental HT29 cells (parent) and HT29 cells transduced with control nontargeting shRNA (control shRNA) or ARPC3-targeting shRNAs (shARPC3-1, shARPC3-2 or shARPC3-3). In **c**, ARPC3 expression was determined by western blotting (left; see also **Supplementary Data Set 1**) and quantitated relative to parental HT29 cells ± s.e.m. (right; $n = 3$ independent western blots). In **d**, cell velocity (μm per minute) relative to parental HT29 cells ± s.e.m. is shown, as measured by time-lapse microscopy ($n = 30$ tracked cells per group pooled from two independent experiments). (**e**) The % replacement (R), % desmoplastic (D) and % pushing (P) HGP per group ± s.e.m. in control- and ARPC3-knockdown tumors ($n = 6$ mice per group). (**f**–**h**) Tumors with normal ARPC3 levels (control shRNA) or ARPC3 knockdown (shARPC3-3) were established in the livers of mice, followed by treatment with B20-4.1.1 plus capecitabine (BC) or vehicle alone (Vh) for 2 weeks. Shown are the % HGP per group ± s.e.m. ($n = 8$ mice per group) (**f**), liver tumor burden expressed in terms of lesion area ± s.e.m. ($n = 8$ mice per group) (**g**) and tumor vessel density expressed in terms of vessels per mm^2 ± s.e.m. ($n = 8$ mice per group) (**h**). For statistical analysis, Student's *t*-test (**c**,**g**,**h**) or Mann–Whitney *U* test (**d**–**f**) were used. $^*P < 0.05$, $^{**}P < 0.01$ $^{***}P < 0.001$, $^{****}P < 0.0001$. n.s., not significant. Scale bars, 50 μM.

BCLMs is presented in **Figure 5b**–**g**. Breast cancer cells colonized the liver by replacing resident hepatocytes (**Fig. 5d**); no desmoplastic stroma was present at the tumor–liver interface (**Fig. 5e**). The vascular architecture of the adjacent liver was preserved at the tumor–liver interface (**Fig. 5f**), and co-option of sinusoidal vessels was observed (**Fig. 5g**). These data show that the replacement HGP, which vascularizes by vessel co-option, predominates in breast cancer liver metastases.

Combined inhibition of vessel co-option and angiogenesis is more effective than inhibition of angiogenesis alone

Vessel co-option in the liver requires the infiltration of cancer cells into the normal liver parenchyma (as observed in **Figs. 3** and **5**). We therefore reasoned that cancer cell motility might be required for vessel co-option. Arp2/3 mediates the nucleation of actin filaments at the leading edge of cells to drive cell movement and has been previously implicated in the motility and invasion of both breast cancer cells and colorectal cancer cells[22–24]. To confirm expression of the Arp2/3 complex in human liver metastases, we performed staining for the Arp2/3 subunit ARPC3 using a well-validated antibody. ARPC3 was expressed in cancer cells in all human specimens examined. Moreover, ARPC3 expression was significantly ($P < 0.04$) higher in replacement HGP metastases, as compared to desmoplastic HGP metastases (**Supplementary Fig. 11**).

To address whether cancer cell motility mediated by Arp2/3 could have a functional role in the process of vessel co-option *in vivo*, we used a preclinical orthotopic model of advanced liver metastasis, in which HT29 colorectal cancer cells are injected directly into mouse liver (**Supplementary Fig. 12**). This model is commonly used to replicate the advanced stage of CRCLM at which patients are treated in the metastatic setting[25–27]. CRCLMs generated in this model had a mixed HGP, composed mainly of replacement HGP areas (**Fig. 6a**), and to a lesser extent, desmoplastic HGP areas (**Fig. 6b**), thus recapitulating the two prevalent HGPs observed in human CRCLMs. We then attempted to knock down ARPC3 expression in HT29 cells using three different ARPC3-targeting shRNA oligonucleotides. Two of these oligonucleotides (shARPC3-2 and shARPC3-3) significantly reduced ARPC3 expression in cells, whereas the third oligonucleotide (shARPC3-1), as well as a control nontargeting oligonucleotide (control shRNA), did not (**Fig. 6c**). ARPC3 knockdown significantly suppressed the migration of HT29 cells (**Fig. 6d**), with no potentially confounding effects on cell proliferation (**Supplementary Fig. 13**).

Notably, ARPC3 knockdown significantly decreased the replacement HGP *in vivo*, while significantly increasing the desmoplastic HGP (**Fig. 6e**). These data indicate that the suppression of Arp2/3-mediated cancer cell motility inhibits the replacement HGP in the context of this model, which blocks the ability of these tumors to co-opt pre-existing liver vessels *in vivo*.

We next evaluated whether combined inhibition of vessel co-option and angiogenesis is more effective at limiting tumor growth than angiogenesis inhibition alone. Mice with established control- or ARPC3-knockdown tumors were treated with a combination of the VEGFA inhibitory antibody B20-4.1.1 (ref. 28) and capecitabine (**Fig. 6f–h**). In control tumors, which have a predominantly replacement HGP (**Fig. 6f**), no significant inhibition of tumor burden was observed in response to treatment, as compared to vehicle control (**Fig. 6g**). However, in ARPC3-knockdown tumors, which have a predominantly desmoplastic HGP (**Fig. 6f**), tumor burden was significantly suppressed by treatment (**Fig. 6g**). In addition, although treatment with B20-4.1.1 in addition to capecitabine led to a reduced tumor vessel density in both control- and ARPC3-knockdown tumors, this effect was more pronounced when vessel co-option was suppressed by knockdown of ARPC3 (**Fig. 6h** and **Supplementary Fig. 14**). The administration of capecitabine alone did not significantly suppress tumor burden or tumor vessel density in either control- or ARPC3-knockdown tumors (**Supplementary Fig. 15**). These data suggest that simultaneous inhibition of angiogenesis and vessel co-option might be a more effective strategy for the treatment of advanced liver metastases than current strategies that target angiogenesis alone.

DISCUSSION

When cancers metastasize to highly vascular organs (including the liver), they can utilize vessel co-option, instead of angiogenesis, as a mechanism to obtain a vascular supply[10]. Here we addressed whether vessel co-option could be a significant mechanism of resistance to anti-angiogenic therapy in patients with colorectal cancer liver metastases. We found that (i) vessel co-option is the predominant mechanism of vascularization in approximately 40% of the lesions that we examined; (ii) metastases that use vessel co-option respond poorly to bev–chemo; (iii) vessel co-option is prevalent in patients who progress after treatment with bev–chemo; and (iv) individuals with metastases that use vessel co-option obtain less clinical benefit from bev–chemo treatment in terms of overall survival. These observations strongly suggest that vessel co-option can blunt the therapeutic benefit of anti-angiogenic therapy in metastatic colorectal cancer.

Our findings also have relevance for breast cancer. Phase 3 trials of bevacizumab combined with chemotherapy in metastatic breast cancer have consistently failed to demonstrate a survival benefit for the addition of bevacizumab[29–33]. Here we found that the majority of breast cancer liver metastases utilize vessel co-option. In addition, vessel co-option occurs in breast cancer metastases to the lymph nodes[34,35], skin[36], lungs[7,37,38] and brain[39–41]. The prevalence of vessel co-option in breast cancer could explain, at least in part, why anti-angiogenic therapy has been a disappointing therapeutic approach to metastatic breast cancer.

Biomarkers that are predictive of response to anti-angiogenic therapy in patients remain elusive[6,11,42]. Given that our data suggest that patients who present with desmoplastic HGP liver metastases might derive more benefit from bevacizumab than patients who present with replacement HGP liver metastases, we propose that the HGP might have potential as a predictive biomarker for anti-angiogenic therapy. A previously published pilot study has shown that, when magnetic resonance imaging (MRI) of the liver is performed immediately after the injection of contrast agent, the presence of transient perilesional enhancement on the MRI image is correlated with increased thickness of the tumor border on histopathological examination, which includes the presence of a peritumoral desmoplastic reaction and peritumoral vascular proliferation[43]. Although it remains to be validated whether imaging can be reliably used to determine the HGPs of liver metastases, we speculate that MRI or CT imaging of the liver might eventually be exploited to identify those patients with desmoplastic HGP liver metastases who are more likely to benefit from anti-angiogenic therapy.

In the longer term, we propose that therapeutic strategies to block vessel co-option in tumors should be developed. In this regard, we found that knockdown of Arp2/3-mediated cancer cell motility suppresses vessel co-option in a preclinical model of advanced liver metastasis, and that combined inhibition of angiogenesis and vessel co-option is more effective at controlling tumor burden than targeting angiogenesis alone. In line with these findings, acquired resistance to the anti-angiogenic drug sorafenib in hepatocellular carcinoma can occur as a result of increased cancer cell invasion in the liver, which mediates co-option of pre-existing liver vessels[44]. Taken together, these and other data[45–52] suggest a key role for cancer cell motility and invasion in the process of vessel co-option, which might be targeted for blocking vessel co-option in tumors.

METHODS

Methods and any associated references are available in the online version of the paper.

Note: Any Supplementary Information and Source Data files are available in the online version of the paper.

ACKNOWLEDGMENTS

The study was supported by Breakthrough Breast Cancer (which recently merged with the Breast Cancer Campaign to form Breast Cancer Now), NHS funding to the NIHR Biomedical Research Centre at RM/ICR (London), the Liver Disease Biobank (Montreal) and De Stichting tegen Kanker (Antwerp). We thank I. Hart, K. Hodivala-Dilke, C. Isacke, R. Kerbel, A. Tutt and the members of the Liver Metastasis Research Network for their critical comments on the work. We thank Genentech for providing B20-4.1.1, S. Petrillo for assistance with the Liver Disease Biobank, J. Campbell for advice on statistical analysis and M. Balazsi for assistance with digital pathology. For their technical assistance, we thank the staff of the ICR Biological Services Unit and the staff of the Breast Cancer Now Histopathology Core Facility.

AUTHOR CONTRIBUTIONS

S. Frentzas, E.S., V.L.B., P.B.V. and S. Foo performed experiments, collected data, analysed data, provided input on the study design and assisted with interpretation of the data; P.B.V., A.W., Z.G., Y.S. and G.V.D.E. performed histopathological analysis of tissue specimens; E.K., M.R.N., F.D., P.G., T.J.B. and Z.E. provided essential technical assistance with experiments; C.P. and X.T. performed statistical analysis on clinical data; A.S. and A.L. assisted with the retrieval of tissue specimens and the associated clinical data; L.R., J.V.R. and S.V.L. shared unpublished data that were crucial to the successful execution of the study and provided critical comments on the manuscript; A.K., G.B., E.L., H.N. and M.S. provided expert assistance with the analysis of clinical data and critical comments on the manuscript; L.D., D.C. and P.M. provided tissue specimens for the study and critical comments on the design of the study and the writing of the manuscript; A.R.R. conceived of and designed the study, supervised the research and wrote the manuscript.

COMPETING FINANCIAL INTERESTS

The authors declare no competing financial interests.

1. Ferrara, N., Hillan, K.J., Gerber, H.P. & Novotny, W. Discovery and development of bevacizumab, an anti-VEGF antibody for treating cancer. *Nat. Rev. Drug Discov.* **3**, 391–400 (2004).
2. Kerbel, R.S. Tumor angiogenesis. *N. Engl. J. Med.* **358**, 2039–2049 (2008).
3. Hurwitz, H. *et al.* Bevacizumab plus irinotecan, fluorouracil, and leucovorin for metastatic colorectal cancer. *N. Engl. J. Med.* **350**, 2335–2342 (2004).
4. Cunningham, D. *et al.* Bevacizumab plus capecitabine versus capecitabine alone in elderly patients with previously untreated metastatic colorectal cancer (AVEX): an open-label, randomised phase 3 trial. *Lancet Oncol.* **14**, 1077–1085 (2013).
5. Ebos, J.M. & Kerbel, R.S. Antiangiogenic therapy: impact on invasion, disease progression, and metastasis. *Nat. Rev. Clin. Oncol.* **8**, 210–221 (2011).
6. Vasudev, N.S. & Reynolds, A.R. Anti-angiogenic therapy for cancer: current progress, unresolved questions and future directions. *Angiogenesis* **17**, 471–494 (2014).
7. Pezzella, F. *et al.* Angiogenesis in primary lung cancer and lung secondaries. *Eur. J. Cancer* **32A**, 2494–2500 (1996).
8. Vermeulen, P.B. *et al.* Liver metastases from colorectal adenocarcinomas grow in three patterns with different angiogenesis and desmoplasia. *J. Pathol.* **195**, 336–342 (2001).
9. Döme, B., Hendrix, M.J., Paku, S., Tóvári, J. & Tímár, J. Alternative vascularization mechanisms in cancer: Pathology and therapeutic implications. *Am. J. Pathol.* **170**, 1–15 (2007).
10. Donnem, T. *et al.* Vessel co-option in primary human tumors and metastases: an obstacle to effective anti-angiogenic treatment? *Cancer Med.* **2**, 427–436 (2013).
11. Jayson, G.C., Kerbel, R., Ellis, L.M. & Harris, A.L. Antiangiogenic therapy in oncology: current status and future directions. *Lancet* **388**, 518–529 (2016).
12. Adams, R.B. *et al.* Selection for hepatic resection of colorectal liver metastases: expert consensus statement. *HPB (Oxford)* **15**, 91–103 (2013).
13. Van den Eynden, G.G. *et al.* The multifaceted role of the microenvironment in liver metastasis: biology and clinical implications. *Cancer Res.* **73**, 2031–2043 (2013).
14. Stessels, F. *et al.* Breast adenocarcinoma liver metastases, in contrast to colorectal cancer liver metastases, display a non-angiogenic growth pattern that preserves the stroma and lacks hypoxia. *Br. J. Cancer* **90**, 1429–1436 (2004).
15. Gruenberger, B. *et al.* Bevacizumab, capecitabine, and oxaliplatin as neoadjuvant therapy for patients with potentially curable metastatic colorectal cancer. *J. Clin. Oncol.* **26**, 1830–1835 (2008).
16. Chaudhury, P. *et al.* Perioperative chemotherapy with bevacizumab and liver resection for colorectal cancer liver metastasis. *HPB* **12**, 37–42 (2010).
17. Wong, R. *et al.* A multicentre study of capecitabine, oxaliplatin plus bevacizumab as perioperative treatment of patients with poor-risk colorectal liver-only metastases not selected for upfront resection. *Ann. Oncol.* **22**, 2042–2048 (2011).
18. Chun, Y.S. *et al.* Association of computed tomography morphologic criteria with pathologic response and survival in patients treated with bevacizumab for colorectal liver metastases. *J. Am. Med. Assoc.* **302**, 2338–2344 (2009).
19. Shindoh, J. *et al.* Optimal morphologic response to preoperative chemotherapy: an alternate outcome end point before resection of hepatic colorectal metastases. *J. Clin. Oncol.* **30**, 4566–4572 (2012).
20. Boonsirikamchai, P. *et al.* CT findings of response and recurrence, independent of change in tumor size, in colorectal liver metastasis treated with bevacizumab. *AJR Am. J. Roentgenol.* **197**, W1060–W1066 (2011).
21. Van den Eynden, G.G. *et al.* The histological growth pattern of colorectal cancer liver metastases has prognostic value. *Clin. Exp. Metastasis* **29**, 541–549 (2012).
22. Nürnberg, A., Kitzing, T. & Grosse, R. Nucleating actin for invasion. *Nat. Rev. Cancer* **11**, 177–187 (2011).
23. Otsubo, T. *et al.* Involvement of Arp2/3 complex in the process of colorectal carcinogenesis. *Mod. Pathol.* **17**, 461–467 (2004).
24. Iwaya, K. *et al.* Correlation between liver metastasis of the colocalization of actin-related protein 2 and 3 complex and WAVE2 in colorectal carcinoma. *Cancer Sci.* **98**, 992–999 (2007).
25. Kopetz, S. *et al.* Synergistic activity of the SRC family kinase inhibitor dasatinib and oxaliplatin in colon carcinoma cells is mediated by oxidative stress. *Cancer Res.* **69**, 3842–3849 (2009).
26. Nyati, M.K. *et al.* The potential of 5-fluorocytosine/cytosine deaminase enzyme prodrug gene therapy in an intrahepatic colon cancer model. *Gene Ther.* **9**, 844–849 (2002).
27. Gray, M.J. *et al.* Therapeutic targeting of Id2 reduces growth of human colorectal carcinoma in the murine liver. *Oncogene* **27**, 7192–7200 (2008).
28. Liang, W.C. *et al.* Cross-species vascular endothelial growth factor (VEGF)-blocking antibodies completely inhibit the growth of human tumor xenografts and measure the contribution of stromal VEGF. *J. Biol. Chem.* **281**, 951–961 (2006).
29. Miller, K.D. *et al.* Randomized phase III trial of capecitabine compared with bevacizumab plus capecitabine in patients with previously treated metastatic breast cancer. *J. Clin. Oncol.* **23**, 792–799 (2005).
30. Miller, K. *et al.* Paclitaxel plus bevacizumab versus paclitaxel alone for metastatic breast cancer. *N. Engl. J. Med.* **357**, 2666–2676 (2007).
31. Miles, D.W. *et al.* Phase III study of bevacizumab plus docetaxel compared with placebo plus docetaxel for the first-line treatment of human epidermal growth factor receptor 2-negative metastatic breast cancer. *J. Clin. Oncol.* **28**, 3239–3247 (2010).
32. Robert, N.J. *et al.* RIBBON-1: randomized, double-blind, placebo-controlled, phase III trial of chemotherapy with or without bevacizumab for first-line treatment of human epidermal growth factor receptor 2-negative, locally recurrent or metastatic breast cancer. *J. Clin. Oncol.* **29**, 1252–1260 (2011).
33. Brufsky, A.M. *et al.* RIBBON-2: a randomized, double-blind, placebo-controlled, phase III trial evaluating the efficacy and safety of bevacizumab in combination with chemotherapy for second-line treatment of human epidermal growth factor receptor 2-negative metastatic breast cancer. *J. Clin. Oncol.* **29**, 4286–4293 (2011).
34. Naresh, K.N., Nerurkar, A.Y. & Borges, A.M. Angiogenesis is redundant for tumour growth in lymph node metastases. *Histopathology* **38**, 466–470 (2001).
35. Jeong, H.S. *et al.* Investigation of the lack of angiogenesis in the formation of lymph node metastases. *J. Natl. Cancer Inst.* **107**, djv155 (2015).
36. Colpaert, C.G. *et al.* Cutaneous breast cancer deposits show distinct growth patterns with different degrees of angiogenesis, hypoxia and fibrin deposition. *Histopathology* **42**, 530–540 (2003).
37. Breast Cancer Progression Working Party. Evidence for novel nonangiogenic pathway in breast-cancer metastasis. *Lancet* **355**, 1787–1788 (2000).
38. Szabo, V. *et al.* Mechanism of tumour vascularization in experimental lung metastases. *J. Pathol.* **235**, 384–396 (2015).
39. Carbonell, W.S., Ansorge, O., Sibson, N. & Muschel, R. The vascular basement membrane as "soil" in brain metastasis. *PLoS One* **4**, e5857 (2009).
40. Bugyik, E. *et al.* Lack of angiogenesis in experimental brain metastases. *J. Neuropathol. Exp. Neurol.* **70**, 979–991 (2011).
41. Valiente, M. *et al.* Serpins promote cancer cell survival and vascular co-option in brain metastasis. *Cell* **156**, 1002–1016 (2014).
42. Jain, R.K. *et al.* Biomarkers of response and resistance to antiangiogenic therapy. *Nat. Rev. Clin. Oncol.* **6**, 327–338 (2009).
43. Semelka, R.C., Hussain, S.M., Marcos, H.B. & Woosley, J.T. Perilesional enhancement of hepatic metastases: correlation between MR imaging and histopathologic findings-initial observations. *Radiology* **215**, 89–94 (2000).
44. Kuczynski, E.A. *et al.* Co-option of liver vessels and not sprouting angiogenesis drives acquired sorafenib resistance in hepatocellular carcinoma. *J. Natl. Cancer Inst.* **108**, djw030 (2016).
45. Rubenstein, J.L. *et al.* Anti-VEGF antibody treatment of glioblastoma prolongs survival but results in increased vascular cooption. *Neoplasia* **2**, 306–314 (2000).
46. Küsters, B. *et al.* Vascular endothelial growth factor-A(165) induces progression of melanoma brain metastases without induction of sprouting angiogenesis. *Cancer Res.* **62**, 341–345 (2002).
47. Leenders, W.P. *et al.* Antiangiogenic therapy of cerebral melanoma metastases results in sustained tumor progression via vessel co-option. *Clin. Cancer Res.* **10**, 6222–6230 (2004).
48. Pàez-Ribes, M. *et al.* Antiangiogenic therapy elicits malignant progression of tumors to increased local invasion and distant metastasis. *Cancer Cell* **15**, 220–231 (2009).
49. de Groot, J.F. *et al.* Tumor invasion after treatment of glioblastoma with bevacizumab: radiographic and pathologic correlation in humans and mice. *Neuro-oncol.* **12**, 233–242 (2010).
50. Lu, K.V. *et al.* VEGF inhibits tumor cell invasion and mesenchymal transition through a MET/VEGFR2 complex. *Cancer Cell* **22**, 21–35 (2012).
51. Sennino, B. *et al.* Suppression of tumor invasion and metastasis by concurrent inhibition of c-Met and VEGF signaling in pancreatic neuroendocrine tumors. *Cancer Discov.* **2**, 270–287 (2012).
52. Depner, C. *et al.* EphrinB2 repression through ZEB2 mediates tumour invasion and anti-angiogenic resistance. *Nat. Commun.* **7**, 12329 (2016).

ONLINE METHODS

Human samples. Specimens were obtained from patients treated at The Royal Marsden Hospital (RM) in London, at McGill University Health Centre (MUHC) in Montreal and at Gasthuiszusters Antwerpen (GZA) Hospitals St. Augustinus in Antwerp. Informed consent was obtained from all patients. Ethical approval was granted by the local Research Ethics Committee at The Royal Marsden, the McGill University Health Centre Research Ethics Board and by the local Research Ethics Committee of the GZA Hospitals St. Augustinus.

All identified cases of CRC liver metastases (CRCLMs) resected from patients treated preoperatively with a combination of bevacizumab and chemotherapy (bev-chemo) at RM from 2006–12 (101 metastases from 47 patients) were examined. Of these, 59 liver metastases from 33 individuals were eligible for our study correlating HGP with pathological response. A consort diagram illustrates how these 59 cases were selected for inclusion (**Supplementary Fig. 2**). For patient characteristics, see **Supplementary Table 1**. To correlate HGP with morphological response on imaging, 52 lesions from 31 patients were eligible for inclusion (**Supplementary Fig. 2**). To correlate HGP with response by RECIST criteria, all 59 liver metastases from 33 individuals were eligible for inclusion.

All identified CRCLMs resected from patients treated pre-operatively with bev–chemo at MUHC from 2008–14 (191 CRC liver metastases from 65 patients) were examined. Of these, 128 liver metastases from 59 patients were eligible for correlating HGP with pathological response (**Supplementary Fig. 4**). For patient characteristics see **Supplementary Table 3**. For the analysis of new CRCLMs (i.e., lesions that presented only after the initiation of bev–chemo but that were not present on baseline scans), we identified 35 resected lesions from 13 patients treated preoperatively with bev–chemo at MUHC (**Supplementary Fig. 4**). For patient characteristics, see **Supplementary Table 6**. A total of 148 liver metastases from 62 patients treated pre-operatively with bev–chemo were eligible for correlating HGP with overall survival. For the analysis of CRC liver metastases from patients who did not receive pre-operative therapy, we identified 32 lesions from 19 patients at MUHC. For patient characteristics, see **Supplementary Table 7**. For the analysis of CRCLMs from patients treated with chemotherapy alone, all identified cases of CRCLMs resected from patients treated preoperatively with chemotherapy at MUHC from 2008–14 (81 metastases resected from 30 patients) were examined. From this group, a total of 76 liver metastases from 29 individuals were eligible for our study correlating HGP with overall survival.

For breast cancer, all identified breast cancer liver metastasis cases obtained via resection or autopsy at GZA Hospitals St. Augustinus from 2004–15 were examined (17 patients) and all cases were eligible for inclusion in the study. For patient characteristics, see **Supplementary Table 11**.

Therapy administration. Patients receiving treatment with bevacizumab in combination with chemotherapy were treated with one of the following regimens:

CAPOX plus bevacizumab: 21-d treatment cycle consisting of a 15-min intravenous infusion of bevacizumab (7.5 mg per kg) and a 2-h intravenous infusion of oxaliplatin (130 mg per m^2) on day 1, followed by daily oral capecitabine (1,700 mg per m^2) in two divided doses from days 1 to 14.

FOLFOX plus bevacizumab: 14-d treatment cycle consisting of a 10-min intravenous infusion of bevacizumab (5 mg per kg), a 2-h intravenous infusion of oxaliplatin (85 mg per m^2), a 2-h intravenous infusion of folinic acid (400 mg per m^2) with a bolus dose of 5-FU (400 mg per m^2) on day 1, followed by a 48-h continuous intravenous infusion of 5-FU (1,200 mg per m^2 per day).

FOLFIRI plus bevacizumab: 14-d treatment cycle consisting of a 10-min intravenous infusion of bevacizumab (5 mg per kg), a 1-h intravenous infusion of irinotecan (180 mg per m^2), a 1-h intravenous infusion of folinic acid (400 mg per m^2) with a bolus dose of 5-FU (400 mg per m^2) on day 1, followed by a 48-h continuous intravenous infusion of 5-FU (1,200 mg per m^2 per day).

For patients who received chemotherapy alone, most received either FOLFOX or FOLFIRI administered as described above, without the addition of bevacizumab. However, a minority of individuals who received chemotherapy alone received one of the following regimens instead.

FOLFIRINOX: 14-d treatment cycle consisting of oxaliplatin (85 mg per m^2), irinotecan (180 mg per m^2), leucovorin (400 mg per m^2) and 5-FU (400 mg per m^2) followed by a 48-h continuous intravenous infusion of 5-FU (1,200 mg per m^2 per day).

5-FU: 14-day treatment cycle consisting of leucovorin (400 mg per m^2) and 5-FU (400 mg per m^2) followed by a 48-h continuous intravenous infusion of 5-FU (1,200 mg per m^2 per day).

The decision to administer therapy, the type of therapy and the number of cycles were based on the recommendation of the local multidisciplinary team. Patients received oxaliplatin- or irinotecan-based regimens with the addition of bevacizumab preferentially, as long as there were no contra-indications to the administration of bevacizumab, such as uncontrolled hypertension, a history of gastrointestinal perforation, a history of arterial or venous thromboembolic events, a history of significant bleeding, recent surgery or nephrotic syndrome. In cases in which the patient was deemed unsuitable for administration of bevacizumab, the patient received chemotherapy alone.

Scoring HGPs. Sections (4 μm in thickness) were prepared from formalin-fixed, paraffin-embedded (FFPE) liver resection specimens, stained with H&E and then scored for HGP by two pathologists with extensive experience of scoring the HGPs. In brief, the tumor–liver interface was categorized as desmoplastic, pushing or replacement HGP according to the following criteria: desmoplastic HGP, no direct contact between cancer cells and liver parenchyma was observed and the cancer cells were separated from the liver parenchyma by a layer of desmoplastic stroma; pushing HGP, close contact between cancer cells and normal liver tissue was observed, without an intervening desmoplastic stroma. The normal liver was compressed by the tumor and no invasion of cancer cells into the hepatic plates was observed; replacement HGP, close contact between cancer cells and liver parenchyma was observed, without an intervening desmoplastic stroma. Cancer cells had invaded the hepatic plates and replaced the hepatocytes without destroying the vascular architecture of the liver at the tumor–liver interface.

Given that some lesions present with a mixture of different HGPs, the percentage of the tumor–liver interface with a desmoplastic, pushing or replacement HGP was scored in intervals of 5% in all available tissue blocks. Where multiple blocks were available, the mean average score was calculated to produce a single score for % desmoplastic, % pushing and % replacement HGP for each lesion.

In some cases, the invasion of cancer cells into the hepatic plates (which is a defining feature of the replacement HGP and required for vessel co-option) was also accompanied by the compression of the liver parenchyma. These cases were scored as replacement HGP and not pushing HGP. This subtle but important refinement to the criteria for scoring the HGPs helps to explain why, in the current study, the incidence of the replacement HGP in CRC metastases is higher than in some previous studies.

Agreement of HGP scores. The level of intra-observer and inter-observer agreement for scoring the HGPs was tested independently. In brief, two pathologists (observers A and B) scored the HGP (% replacement, % desmoplastic and % pushing) in 150 tissue sections of resected CRCLM without conferring. After a break of several weeks, the two pathologists scored the same set of 150 tissue sections again without conferring and without reference to their previous scores. The % replacement scores from each round of scoring were then used to test the level of intra- and inter-observer agreement. The difference between scores is plotted in **Supplementary Figure 16**.

The correlation between scores was calculated using Pearson's correlation coefficient. We also analyzed the data using Bland–Altman plots (**Supplementary Fig. 17**) from which we determined the mean difference between the scores and the limits of agreement (two s.d. from the mean difference)[53]. The results are tabulated in **Supplementary Table 12**.

There was a strong correlation ($r > 0.98$) between the scores recorded by the same observer (intra-observer agreement) and also a strong correlation ($r > 0.96$) between the scores recorded by the two different observers (inter-observer agreement). The Bland–Altman plots showed that the mean difference between the scores recorded by the same observer was small (0.033 and −0.633) and that the mean difference between the scores recorded by the two different observers was also small (−1.500 and −2.167). Taken together, these data indicate that there is a high level of intra- and inter-observer agreement between observers scoring the HGPs.

Despite this, the limits of agreement for the inter-observer agreement are quite wide (−22.88 to 19.88 and −25.287 to 20.953). This occurred because of

the presence of some cases that have a 'mixed' growth pattern that can be more difficult to score, leading to divergent scores. However, in the main study, for any cases having a 'mixed' growth pattern where there was a substantial disagreement between the two observers, they were always able to reconcile their differences to produce a single consensus score for the lesion.

Scoring of pathological response to therapy. For scoring of the pathological response to bev–chemo from H&E-stained specimens, the extent of viable carcinoma was assessed semi-quantitatively as a percentage relative to the total tumor surface area. Each lesion was assigned to one of four categories: >75%, 50–75%, 25–49% or <25% viable carcinoma[54], with areas of 'usual necrosis' being considered part of the viable tumor fraction, whereas areas of 'infarct-like necrosis' were considered to be nonviable[55]. Pathological response was scored independently by three experienced pathologists using these criteria. Any differences in scores that occurred between pathologists were resolved by consensus to produce a single score for each lesion.

Scoring of morphological response to therapy. Pre- and post-treatment contrast-enhanced CT scans of suitable quality were available for 52 lesions from 31 individuals for this analysis (see consort diagram, **Supplementary Fig. 2**), and the response to therapy was evaluated using a method based on previously published morphological response criteria[18,20], as described below.

The appearance of each lesion on both the pre- and post-treatment scan was scored as belonging to one of three morphology groups (group-1, group-2 or group-3). A homogeneous, low-attenuation lesion with a thin, sharply defined tumor–liver interface was defined as group-1. A lesion having heterogeneous attenuation and a thick, poorly defined tumor–liver interface was defined as group-3. A lesion that was intermediate between group-1 and group-3, having a moderate degree of heterogeneous attenuation and a moderately defined tumor–liver interface was defined as group-2.

Morphological response was defined as an optimal response (OR) if the lesion changed from a group-3 or group-2 to a group-1 after treatment; a partial response (PR) if the lesion changed from group-3 to group-2 after treatment; and an absent response (AR) if the metastasis either did not change group or went from group-2 to group-3 after treatment. Morphological response was scored independently by two observers. Any difference in scores was resolved by consensus to produce a single score for each lesion. Lesions scored as AR were considered to be poor responders, whereas lesions scored as PR or OR were considered to be good responders. Scorers were blinded to the HGP and pathological response data.

Scoring of response by RECIST. The change in lesion size was determined from magnetic resonance imaging (MRI) scan data by calculating the change in lesion diameter that occurred between the pre- and post-treatment scans. The lesion size measurements were obtained from the patient records and were therefore blinded because the original reporting radiologist had no prior knowledge of our retrospective HGP and pathological response data. For this analysis, MRI scans of suitable quality were available for 59 lesions from 33 patients. Lesions were classified as partial response (PR), stable disease (SD) or progressive disease (PD) according to the following criteria: PR (lesion underwent ≥30% decrease in size between pre- and post-treatment scan), SD (lesion underwent <30% decrease in size and <20% increase in size between pre- and post-treatment scan) and PD (lesion underwent ≥20% increase in size between pre- and post-treatment scan).

Kaplan–Meier estimate of overall survival. Patients were allocated to one of three groups: predominant replacement, predominant desmoplastic or predominant pushing. To allocate patients to each group, the mean percentage of replacement, desmoplastic and pushing HGP was calculated for each patient using the data available from all lesions. Patients with a mean replacement HGP of >50% were allocated to the predominant replacement group, patients with a mean desmoplastic HGP of >50% were allocated to the predominant desmoplastic group and patients with a mean pushing HGP of >50% were allocated to the predominant pushing group. This method allowed for unambiguous allocation of patients to the three groups (i.e., there were no patients scored as having a 50:50 score for two growth patterns). Overall survival estimates were calculated from the date of diagnosis of liver metastases to the date of death or to the date of last follow-up.

Immunohistochemistry. Sections 4 μm in thickness were prepared from FFPE blocks, de-paraffinized and rehydrated by standard protocols. Depending on the antibodies used, antigen retrieval was performed either at pH 6 in a pressure cooker (Menapath Access Retrieval Unit, Menarini Diagnostics) or at pH 9 in a microwave. Sections were incubated in blocking buffer (1% BSA in PBS-T) for 1 h, followed by incubation with primary antibodies in blocking buffer for 2 h, all at room temperature. Primary antibodies used were: mouse anti-ARPC3 (Millipore, MABT95; dilution 1:2,500), mouse anti-human CD31 (Dako, M0823; dilution 1:30), rabbit anti-mouse CD31 (Dianova, DIA310; dilution 1:75), rabbit anti-collagen-3 (Abcam, ab7778; dilution 1:200), mouse anti-cytokeratin-19 (Dako, M0888; dilution 1:100), mouse anti-cytokeratin-20 (Dako, M7019; dilution 1:50), mouse anti-estrogen receptor-α (ER) (Dako, M3643, dilution 1:80), mouse anti-hepatocyte specific antigen (Santa Cruz Biotechnology, sc-58693; dilution 1:400), mouse anti-pan-cytokeratin (Dako, M3515, dilution 1:75), rabbit anti-pan-cytokeratin (Dako, Z0622; dilution 1:400), mouse anti-Ki67 (Dako, M7240; dilution 1:300), mouse anti-progesterone receptor (PgR) (Dako, M3643; dilution 1:200) and rabbit anti-α-SMA (Abcam, ab5694; dilution 1:500). Antibody validation is provided on the manufacturers' websites. For immunofluorescence, primary antibodies were detected with Alexa-488 or Alexa-555 fluorescently conjugated secondary antibodies (Invitrogen) diluted in blocking buffer supplemented with DAPI for 30 min at room temperature, followed by mounting under glass coverslips in MOWIOL mountant supplemented with anti-fade (0.1% w/v 1,4-diazabicyclo[2.2.2]octane) (Sigma-Aldrich). For DAB and TMB staining, primary antibodies were detected with Envision Flex system (K8002, Dako), followed by a light counterstain with hematoxylin before being mounted under glass coverslips in DPEX mountant. For HER2 we used the HercepTest kit (SK001, Dako). Images were captured using a confocal laser-scanning microscope (Leica) or a light microscope (Olympus), as appropriate.

Scoring subtypes of breast cancer. Cases of breast cancer liver metastasis were characterized for intrinsic molecular subtype as per published guidelines[56]. In brief, FFPE sections were stained for ER, PgR, HER2 or Ki67 and scored by a pathologist. For both ER and PgR, positive staining in ≥1% of tumor cell nuclei was required for the case to be considered receptor positive[57]. For HER2, the following system was used: 0 or 1^+ ($HER2^-$), 2^+ (HER2 borderline) or 3^+ ($HER2^+$)[58]. HER2 borderline cases underwent additional testing using the HER2 CISH pharmDx kit (SK109, Dako) to test for HER2 amplification. The presence of HER2 amplification was considered to indicate that the case was HER2 positive. Cases were deemed Ki67 'low' if <14% of nuclei were Ki67 positive; otherwise, they were considered to be Ki67 'high.' The results of the ER, PgR, HER2 and Ki67 analysis were then used to assign each case to an intrinsic molecular subtype according to the criteria recommended by Goldhirsch *et al.*[56], as detailed in **Supplementary Table 13**.

Cell culture. Luciferase-tagged HT29 cells (HT-29-luc2 from Caliper Life Sciences) were authenticated by STR typing and regularly tested for mycoplasma and shown to be contamination free. They were cultured in DMEM supplemented with 10% FCS, L-glutamine and penicillin/streptomycin at 37°C in an atmosphere of 5% CO_2.

shRNA knockdown. HT29 cells were stably transduced with shRNA oligonucleotides using lentiviral particles. We used three different shRNA oligonucleotides designed to target ARPC3 (shARPC3-1, shARPC3-2, shARPC3-3) and a control oligonucleotide with a validated non-targeting sequence (control shRNA) as follows: shARPC3-1 (5′CACCCGCTTAATAAGAATAAGTACGAATACTTATTCTTATTAAGCG3′); shARPC3-2 (5′CACCGAAATGTATACGCTGGGAATCCGAAGATTCCCAGCGTATACATTTC3′); shARPC3-3 (5′CACCGCCAAGGTGAGAAAGAAATGTCGAAACATTTCTTTCTCACCTTGGC3′); control shRNA (5′CACCTAAGGCTATGAAGAGATACCG AAGTATCTCTTCATAGCCTTA3′).

Oligonucleotides were ligated into the pENTR/U6 Gateway system entry vector (Invitrogen), according to the manufacturer's instructions. Oligonucleotide

doi:10.1038/nm.4197

sequences were verified by sequencing and then transferred, together with the U6 promoter, into the Gateway-modified pSEW lentiviral vector (this vector also contains the EGFP gene under the control of an independent SFFV promoter). Viral supernatants were generated by lipofectamine-2000 co-transfection of this expression vector and two packaging vectors (psPAX2 and pMD2.G) into HEK293T cells. Viral supernatants were collected and stored at −80 °C until use. Adherent HT29 cells were infected with viral supernatant for 24 h. After this, the infecting medium was aspirated and replaced by DMEM complete. At 3–5 d after infection, HT29 cells were trypsinized and sorted for GFP expression by flow cytometry on a FACS ARIA instrument (BD Biosciences).

Western blotting. Western blotting was performed as described[59]. In brief, cell lysates were separated on 10% SDS–PAGE gels at 150 V for 1 h. Transfer to nitrocellulose membranes was performed at 100 V for 1 h. Membranes were blocked using blocking buffer (TBS-T supplemented with 5% milk) and then probed with anti-ARPC3 antibodies (Santa Cruz Biotechnology, sc-136020; dilution 1:200) or anti-HSC70 antibodies (Santa Cruz Biotechnology, sc-7298; dilution 1:20,000). After incubation with HRP-conjugated secondary antibodies in blocking buffer, membranes were incubated with chemiluminescence substrate and exposed to film. Densitometry was performed using ImageJ software on three independent western blots. Expression levels of ARPC3 were normalized to the expression level of HSC-70. Antibody validation is provided on the manufacturer's website.

Cell motility assay. Cells were plated at a density of 50,000 cells per well in a 6-well plate. After 24 h, the media was refreshed and the plates were transferred to the stage of an inverted Leica IX-70 time-lapse microscope at 37°C in an atmosphere containing 5% CO_2. Images were captured through a 20× phase-contrast objective every 30 min for 48 h. To measure cell migration, random cells were tracked in time-lapse videos for 30 h using the manual-tracking plugin in ImageJ. For the purposes of quantification, 30 cells from each experimental group were analyzed from across two independent experiments. Results were expressed in terms of cell velocity (μm per minute).

Cell proliferation assay. To assess the proliferation kinetics of cells, 2,000 HT29 cells were seeded (in quadruplicate wells) into four different 96-well plates (plates 1 to 4). Cell viability was measured from plates 1, 2, 3 and 4 at 24, 48, 72 and 96 h, respectively, using the CellTiter-Glo reagent (Promega) according to the manufacturer's instructions. The quantity of viable cells at 48 h, 72 h and 96 h was expressed relative to the quantity of viable cells at 24 h from three independent experiments.

Preclinical model of advanced liver metastasis. The Institute of Cancer Research Animal Ethics Committee granted approval for animal work. Procedures were performed in accordance with United Kingdom Home Office regulations. We used female CB17 SCID mice (CB17/lcr-*Prkdc*^{scid}/lcrlcoCrl) at 12–16 weeks of age (obtained from Charles River UK). Parental HT29 cells, or HT29 cells stably transduced with shRNA constructs, were re-suspended in growth-factor-reduced Matrigel (Invitrogen) at a concentration of 1×10^7 cells per ml. Cells were introduced into the liver by laparotomy performed under general anesthesia (inhaled isofluorane). A midline incision was made through the peritoneum and the left main lobe of the liver was exteriorized. This lobe was injected with 4×10^5 cells in a volume of 40 μl using a 29-gauge needle and then returned to the peritoneal cavity, followed by closure of the wound. To assess the effect of ARPC3 knockdown on the HGP (**Fig. 6e**), mice were culled 21 d after injection of cancer cells. The tumor-bearing liver lobe was harvested, fixed in formalin and embedded in paraffin.

For experiments in which treatment was administered (**Fig. 6f–h** and **Supplementary Fig. 15**), we waited for 10 d after injection to allow for tumor establishment. At 10 d, mice were injected subcutaneously with 75 mg per kg of D-luciferin (Caliper Life Sciences), anesthetized with isofluorane and then imaged in an Lumina II IVIS (*in vivo* Imaging System) instrument (Caliper Life Sciences). Quantification of liver bioluminescence was performed using Living Image software (Caliper Life Sciences) according to manufacturer's instructions. The bioluminescence measurement was used to ensure that subjects of equivalent tumor burden were allocated to each experimental group.

Capecitabine powder (LC Laboratories) was dissolved in vehicle for oral administration (40 mM citrate buffer pH 6, 5% gum Arabic). B20-4.1.1 (Genentech), an antibody that blocks both mouse and human VEGFA[28], was formulated in sterile PBS for intraperitoneal administration. One cycle of therapy consisted of the following: mice received 500 mg per kg capecitabine or vehicle by oral gavage every day for 5 d, followed by a 2 d treatment break, with intraperitoneal injection of 2.5 mg per kg B20-4.1.1 or vehicle on the first and fifth day of the cycle. In mice that received capecitabine alone, the same protocol was followed but without the administration of B20-4.1.1. Mice were given two cycles of therapy and then culled at 24 d after the injection of cancer cells. The tumor-bearing liver lobe was harvested, fixed in formalin and embedded in paraffin.

For quantification of tumor burden, H&E-stained sections were prepared. Sections were digitally scanned (Nanozoomer, Hamamatsu) and imported into NDPI viewer software (Hamamatsu). The marquee tool was used freehand to create regions of interest (ROIs) around areas of tumor in the section, and tumor burden measurement was calculated in terms of area in mm^2. For quantification of vessel density, sections were co-stained for CD31 (detected with TMB) and CK20 (detected with DAB). Tumor vessels were manually counted and expressed in terms of vessels per mm^2 of tumor area. H&E-stained sections were scored for HGP according to the same criteria used for human samples of liver metastasis. The scoring of tumor burden, vessel density and HGPs was performed in a blinded fashion. The number of mice per group was selected on the basis of prior experience regarding the minimum number of animals necessary to detect a statistically significant difference between experimental groups. No randomization method was used.

ARPC3 staining. HT29 cells stably transfected with the control shRNA or shARPC3-3 were grown to confluency, washed in PBS, harvested by trypsinization and then pelleted by centrifugation. Pelleted cells (approximately 1×10^7 cells per pellet) were then resuspended in formalin and fixed for 15 min, which was followed by pelleting again and embedding in paraffin. Tissue sections were prepared and then stained using anti-ARPC3 antibody (Millipore, MABT95; dilution 1:2,500) as described above (see 'Immunohistochemistry') with antigen retrieval performed in pH 6 citrate buffer by heating in a microwave for 18 min.

The same staining protocol was used to stain for ARPC3 in FFPE tissue sections of human liver metastasis specimens. Positive staining for ARPC3 was observed in cancer cells and in some stromal cell types (including immune cells and Kuppfer cells), but only cancer cell staining was scored. The scoring of ARPC3-staining intensity in cancer cells was performed semi-quantitatively by a pathologist. For each case examined, the percentage of cancer cells having 1^+ (weak), 2^+ (moderate) or 3^+ (strong) staining intensity was scored. The result for each case was expressed as an H-score as calculated by the formula: (% area of weak staining) + (2× % area of moderate staining) + (3× % area of strong staining). This generated a score between 0 and 300 for each case.

Statistical analysis. The univariate analysis of clinical data reported in **Figures 1** and **2**, **Supplementary Figures 3** and **5–8** and **Supplementary Tables 2**, **4**, **9** and **10** was performed using the two-tailed χ^2 test. A univariate and multivariate analysis on 181 lesions from 90 patients was performed to determine clinical characteristics that were significantly associated with a good pathological response. Given that some lesions came from the same patient, a generalized estimating equation (GEE) approach was used to account for the within-patient covariance (an exchangeable working correlation structure was used to specify the correlation among lesions clustered within the same patient). A total of 12 different clinical variables were included in the univariate analysis. Only five variables that met a pre-defined threshold for association with pathological response in the univariate GEE analysis ($P < 0.25$) were then included in the subsequent multivariate GEE analysis. The results of the analysis are reported in **Supplementary Table 5**.

For the overall survival data, the log–rank test was used to determine the statistical significance, and Cox proportional hazards regression was used to determine hazard ratios (**Fig. 4b–e**). A univariate and multivariate analysis to determine clinical characteristics associated with overall survival was performed using the Cox proportional hazards regression model. A total of 12 different

clinical variables were included in the univariate analysis. Only two variables that met a pre-defined threshold for association with overall survival in the univariate analysis ($P < 0.25$) were then included in the subsequent multivariate analysis. The results of the analysis are reported in **Supplementary Table 8**. The proportional hazards assumption for the Cox regression models was tested on the basis of weighted Schoenfeld residuals[60]: for the overall survival analyses (**Fig. 4b–e**), the *P* values calculated ranged from 0.09 to 0.69, and for the univariate analyses, the *P* values calculated ranged from 0.08 to 0.99 (depending on the variable), whereas the global *P* value calculated for the multivariate analysis was 0.85, indicating that the proportional hazards ratio assumption was not rejected in any instance.

Where appropriate, the Kolmogorov–Smirnov normality test was used to determine the normality of the data and the F-test equality of variances test was used to determine whether the variance between groups was similar. For normally distributed data, we used two-tailed unpaired Student's *t*-test (with Welch's correction applied if the variance between groups was not similar) to compare experimental groups (**Fig. 6g**,**h** and **Supplementary Figs. 11h** and **15b**,**c**). For non-normally distributed data, we used the Kruskal–Wallis test (**Fig. 4a**) or Mann–Whitney *U*-test (**Fig. 6d–f** and **Supplementary Fig. 15a**) to compare experimental groups. For data where the sample number was too small ($n = 3$ independent experiments) to determine normality, but where the variance between groups was similar, we used two-tailed unpaired Student's *t*-test to compare experimental groups (**Fig. 6c** and **Supplementary Fig. 13**). Intra- and inter-observer agreement for scoring the HGPs was analyzed using Pearson's correlation co-efficient and Bland–Altman plots (**Supplementary Fig. 17**). For all statistical analyses, *P* values below 0.05 were considered to be statistically significant.

53. Bland, J.M. & Altman, D.G. Statistical methods for assessing agreement between two methods of clinical measurement. *Lancet* **1**, 307–310 (1986).
54. Ribero, D. *et al.* Bevacizumab improves pathologic response and protects against hepatic injury in patients treated with oxaliplatin-based chemotherapy for colorectal liver metastases. *Cancer* **110**, 2761–2767 (2007).
55. Chang, H.H., Leeper, W.R., Chan, G., Quan, D. & Driman, D.K. Infarct-like necrosis: a distinct form of necrosis seen in colorectal carcinoma liver metastases treated with perioperative chemotherapy. *Am. J. Surg. Pathol.* **36**, 570–576 (2012).
56. Goldhirsch, A. *et al.* Personalizing the treatment of women with early breast cancer: highlights of the St Gallen International Expert Consensus on the Primary Therapy of Early Breast Cancer 2013. *Ann. Oncol.* **24**, 2206–2223 (2013).
57. Hammond, M.E. *et al.* American Society of Clinical Oncology/College of American Pathologists guideline recommendations for immunohistochemical testing of estrogen and progesterone receptors in breast cancer (unabridged version). *Arch. Pathol. Lab. Med.* **134**, e48–e72 (2010).
58. Wolff, A.C. *et al.* Recommendations for human epidermal growth factor receptor 2 testing in breast cancer: American Society of Clinical Oncology/College of American Pathologists clinical practice guideline update. *J. Clin. Oncol.* **31**, 3997–4013 (2013).
59. Gourlaouen, M., Welti, J.C., Vasudev, N.S. & Reynolds, A.R. Essential role for endocytosis in the growth factor-stimulated activation of ERK1/2 in endothelial cells. *J. Biol. Chem.* **288**, 7467–7480 (2013).
60. Grambsch, P.M. & Therneau, T.M. Proportional hazards tests and diagnostics based on weighted residuals. *Biometrika* **81**, 515–526 (1994).

doi:10.1038/nm.4197